Desalination and Water Treatment
www.deswater.com
doi: 10.1080/19443994.2013.878255

54 (2015) 113–121
April

Taylor & Francis
Taylor & Francis Group

Adsorption of sulfamonomethoxine antibiotics to cucurbit[6]uril polymer: kinetics and thermodynamic studies

Hong-Tao Qiao[a,b], Yun Liu[a,*], Yuan-Hua Dong[a], Sirui Li[c], Ping Wang[b], Tao Jin[a]

[a]*Key Laboratory of Soil Environment and Pollution Remediation, Institute of Soil Science, Chinese Academy of Sciences, Nanjing 210008, China*
Tel. +86 25 86881370; Fax: +86 25 86881000; email: yliu@issas.ac.cn
[b]*School of Chemistry and Biological, Lanzhou Jiaotong University, Lanzhou 730070, China*
[c]*Nanjing Foreign Language School, Nanjing 210008, China*

Received 2 September 2013; Accepted 16 December 2013

ABSTRACT

The occurrence of sulfonamide antibiotics in aquatic environments has been recognized as a significant issue warranting focused attention. A cucurbituril polymer (CP) was used as an adsorbent for sulfamonomethoxine (SMM) in aqueous solution. The experimental isotherm data were analyzed using non-linear Freundlich and Henry isotherm equations. Five error functions were used to predict the parameters of the isotherm. The Freundlich model had performed better with respect the equilibrium data and the HYBRID error function provided the lowest sum of normalized error. Our thermodynamic investigation indicated that the adsorption of SMM onto CP was spontaneous at all temperatures and was an exothermic process. The pseudo-first-order and pseudo-second-order kinetic model were used to fit the kinetics process of SMM adsorption on CP. The adsorption of SMM could be best described by the pseudo-second-order equation. The intra-particle diffusion model was used to further analyze the diffusion mechanism of SMM on CP. The result implies that intra-particle diffusion is not the only rate-limiting step. And the adsorption was favorable in the pH range of 2.0–6.0. The results indicate that CP could serve as alternative adsorbent for removing SMM antibiotics from water.

Keywords: Polymer; Cucurbiturils; Sulfamonomethoxine; Adsorption

1. Introduction

Sulfonamide antibiotics are widely used and produced in large quantities for the treatment of bacterial, protozoal, and fungal infections in humans, animals, and aquatic organisms [1]. Sulfonamide antibiotics and its metabolites are refractory compounds; municipal sewage treatment plants cannot effectively eliminate sulfonamides [2]. In many countries, antibiotics have been detected in surface water, groundwater, and soil [1,3,4]. In addition, sulfonamides are among the most frequently detected antibiotics [5]. Sulfonamide antibiotics are also potentially toxic to aquatic organisms. These toxic substances may eventually reach humans through the food chain and drinking water [6,7]. However, the removal of antibiotics by existing water treatment technologies is incomplete. Thus, there is a need for adequate treatment of sulfonamide antibiotics. Many

*Corresponding author.

studies have shown that sulfonamide antibiotics may be removed by adsorption methods, such as those based on multivalent carbon nanotubes, activated carbon, and activated sludge, natural soil, humic substance, ferrihydrite, and clay mineral [8–13].

Cucurbit[*n*]uril (CB[*n*]) are a new family of molecular hosts comprising *n* glycoluril units, a hydrophobic cavity and two identical carbonyl-laced portals [14]. The isolation and characterization of the first member of this family, cucurbit[6]uril was reported in 1981 by Mock [15], which allow it to form stable host–guest complexes with several different types of guests in its hydrophobic cavity because of a combination of non-covalent interactions including the hydrophobic effect, ion–dipole interactions, and hydrogen bonding [16]. Cucurbituril as adsorbent for the removal of reactive dyes has been reported [17,18]. However, acids and cations in water increase the solubility of CB[6]; thus, CB[6] cannot be used as a sorbent. Hence, Karcher proposed that CB[6] should be attached to a carrier in order to produce a useful sorbent [18]. Our team has used cucurbit[6]uril-anchored silica gel (ACB[6]-SG) as adsorbent for sulfamonomethoxine (SMM) [19]. The anchored cucurbituril was prepared by mixing 0.1 g perallyloxyCB[6] (ACB[6]) with MSG (5.0 g) under an electrodeless microwave lamp light. The adsorption of SMM onto ACB[6]-SG reached equilibrium in 2 min. The adsorption of SMM onto ACB[6]-SG was studied at 278, 298, and 318 K, and lower temperatures favored higher adsorption efficiencies. The adsorption of SMM on ACB[6]-SG could be well described by both the Henry model and the Freundlich model. And we also prepared cucurbituril polymer (CP) using photoinitiated thiol-ene reaction between perallyloxyCB[6] and 1,2-Ethanedithiol with a facile method under microwave electrodeless lamps [20], which FT-IR spectrum revealed two characteristic peaks of CB[6] unit of the C=O and C–N stretching vibrations, and the product is similar to that obtained under ordinary UV light by Jon et al. [21]. We hope to find the new usage of this polymer in the environmental remediation.

In the present study, the focus of the research was to explore the feasibility of using CP as an effective adsorbent for SMM removal from contaminated water bodies. Five different error functions were examined and the isotherm parameters were critically assessed by minimizing the individual error function with the aid of a solver add-on in Microsoft's Excel 2007 (Microsoft Corporation). The Freundlich and Henry isotherms were used to discuss this issue. The thermodynamic parameters (the Gibbs free energy (ΔG), heat of adsorption (ΔH), and entropy change (ΔS)) of the adsorption were determined. The kinetic data and equilibrium data of adsorption studies were processed in order to understand the adsorption mechanism of SMM onto CP. The effect of pH on SMM adsorption was also investigated.

2. Experimental sections

2.1. Materials

PerallyloxyCB[6] used in the experiments were synthesized in our laboratory [21,22]. SMM was purchased from Sigma–Aldrich (USA).

2.2. Preparation of CP [20]

1,2-Ethanedithiol (0.05 mL) was added to a solution of (allyloxy)12cucurbit[6]uril (0.0520 g) in methanol (50 mL). After purging with N_2, an electrodeless lamp was put in flat bottom flasks and hung from a rack. The mixture was irradiated by UV light from a microwave (100 mA) energy-saving lamp for 30 min. The product was filtered, washed by ethanol two to three times, and then dried in a vacuum oven at 75°C.

2.3. Analytical methods

The SMM concentration in the solution was measured by high-performance liquid chromatography (HPLC) on a Waters Alliance 2695 separation module equipped with a Waters 2996 photodiode array detector and Millennium^{32} software. The chromatographic column used was a Gemini C_{18} (150 × 4.6 , 5 μm), and the protection column was a Gemini C_{18} (4.0 × 3.0 mm i.d.). The mobile phase consisted of HAc–NaAc buffer (0.02 mM L^{-1}, pH 4.75): acetonitrile (80:20). The detection wavelength was 268 nm, the flow rate was 0.8 mL/min, and the column temperature was 30°C.

2.4. Batch kinetic studies

The adsorption of SMM was performed by shaking 0.0200 g of adsorbent in 25 mL of SMM solution (0.8 and 4.0 mg/L) in a 40 mL EPA sample bottle equipped with polytetrafluoroethylene-lined screw caps at 150 rpm; the experiment was performed at 298 K. At specific time intervals, samples of each SMM solution were obtained by using a 2 mL syringe with a 0.45 μm stream filter head. Leachate was used for determination of SMM concentration using HPLC. The adsorption amount to be calculated with the following formula:

$$q_t = \frac{(C_0 - C_t)V}{M} \quad (1)$$

where C_0 is the initial concentration (mg/L) of SMM, C_t is the concentration (mg/L) of SMM at time t, M is the quality of the adsorbent (0.0200 g), and V is the volume of SMM solution (25 mL).

2.5. Batch adsorption

A series of 0.0200 g of CP were put into 25 mL of SMM solution at concentrations of 0.5–4.0 mg/L at an initial pH of 5.68. All solutions were stored in 40 mL EPA vials equipped with polytetrafluoroethylene-lined screw caps at the 288, 298, and 313 K. The vials were covered with aluminum foil to prevent photodegradation, and shaken for 48 h at 150 rpm. Afterward, the solution was filtered using 2 mL disposable syringes and 0.22 μm filter membranes. The concentration of SMM in the solution was determined by HPLC.

Separate sets of experiments were conducted to test the effects of pH. A series of SMM solutions were prepared by adjusting the pH to 2.0–12.0 using hydrochloric acid and sodium hydroxide solutions.

3. Results and discussion

3.1. Adsorption kinetics

The kinetic adsorption of SMM by CP is shown in Fig. 1. The figure reveals that increased time increased the uptake of SMM, and attained equilibrium in 20 h. Adsorption kinetics models are used to explain adsorption mechanism and adsorption characteristics.

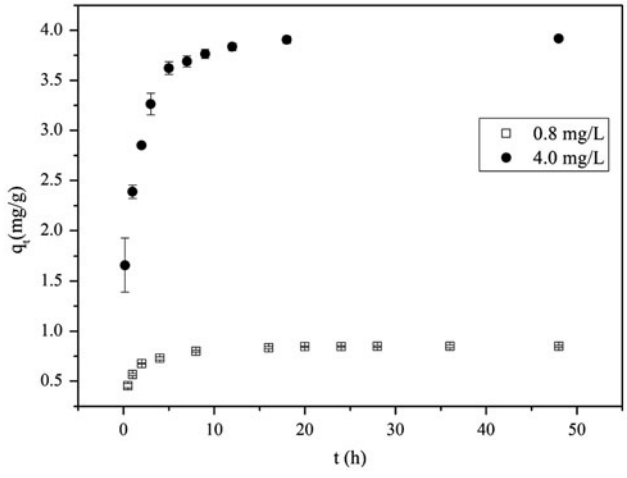

Fig. 1. Adsorption kinetic of SMM on CP.

Pseudo-first-order and pseudo-second-order equations were used. The adsorption kinetics rate of SMM on CP was calculated using kinetics models at initial concentration of 0.8 and 4.0 mg/L. A comparison was performed by utilizing the experimental data, calculated data, and the regression correlation coefficient (R^2).

The pseudo-first-order kinetic model has been widely used to predict dye adsorption kinetics. A linear form of the pseudo-first-order model was described by Lagergren, and it follows [23]:

$$\ln(q_e - q_t) = \ln q_e - k_1 t \quad (2)$$

where q_t is the amount adsorbed at time t (mg/g), q_e is the amount adsorbed at equilibrium (mg/g), and k_1 is the equilibrium rate constant of the pseudo-first-order adsorption (h^{-1}).

The plot ln ($q_e - q_t$) vs. time gave fairly straight lines with the calculated q_e, k_1, and the corresponding linear regression correlation coefficient R^2 values which are shown in Table 1. This plot has a low correlation coefficient with the experimental data, and the calculated q_e value does not agree with the experimental results. This shows no applicability of the pseudo-first-order model in predicting the kinetics of SMM adsorption on CP.

The kinetics data were further analyzed using pseudo-second-order kinetics, represented by [23]:

$$\frac{t}{q_t} = \frac{1}{h} + \frac{t}{q_e} \quad (3)$$

where $h = k_2 q_e^2$ can be regarded as the initial sorption rate as $t \to 0$, and k_2 is the pseudo-second-order rate constant (g/mg/h). The plot t/q_t vs. t should give a straight line if pseudo-second-order kinetic is applicable and q_e, k_2, and h can be determined from the slop and intercept of the plot, respectively.

The calculated q_t, k_2, and the corresponding linear regression correlation coefficient R^2 values are summarized in Table 1. In the pseudo-second-order kinetics, the calculated q_t values are nearly the same as the experimental values, and the regression coefficients are greater than 0.99, indicating that the adsorption phenomena follow pseudo-second-order kinetics. This indicates that SMM on the CP adsorption system obeys the pseudo-second-order kinetic model for the entire sorption period. The data also showed that the initial SMM concentrations influenced the contact time necessary to reach equilibrium and that the sorption capacity increased for the higher initial SMM concentrations. And the initial sorption rate h and

Table 1
Pseudo-first and pseudo-second order parameters and correlation coefficients calculated from experimental data

		Pseudo-first-order model			Pseudo-second-order model			
C_0	q_{cal}	q_e	k_1	R^2	q_e	h	k_2	R^2
4.0	3.9183	1.7971	0.2770	0.9798	3.9683	7.7399	0.4915	0.9999
0.8	0.8469	0.1680	0.0780	0.7374	0.8590	1.6861	2.2850	0.9999

pseudo-second-order rate constant k_2 are increased with increase in initial SMM concentration.

Usually, any sorption process is comprised of several steps, involving transport of the solute molecules from the aqueous phase to the surface of the solid particulates (film diffusion), diffusion of the solute molecules into the interior of the pores, and sorption onto interior sites. Among those steps, the first, sharper region is the instantaneous adsorption or external surface adsorption. The second region is the gradual adsorption stage where intra-particle diffusion is the rate limiting [24]. In some cases, the third region exists which is the final equilibrium stage. If intra-particle diffusion is the rate-controlling factor, uptake of the adsorbate varies with the square root of time, which has been reported by Weber and Morris [25]. They also gave the intra-particle diffusion rate constant equation as follows:

$$q_t = k_i t^{0.5} + C_i \quad (4)$$

where k_i (mg/g h$^{0.5}$), the rate parameter of stage i, is obtained from slope of the straight line of q_t vs. $t^{0.5}$. C_i is the intercept which is the boundary layer, and gives an idea about the thickness of boundary layer, i.e. the larger the intercept, the greater the boundary layer effect.

Fig. 2 presents the plots of q_t vs. $t^{0.5}$ for SMM adsorption. Based on the figures, the data are not linear over the whole adsorption time, showing that the adsorption of SMM on CP does not agree with intra-particle diffusion over the entire adsorption time. However, it is also observed that the sorption process tends to be followed by multi-linearity. This indicates that two or more steps occur in the adsorption process, and the intra-particle diffusion gives a good simulation within the corresponding adsorption period. However, every linear line does not pass through the origin, indicating that intra-particle diffusion is involved in the adsorption process but it is not the only rate-limiting mechanism and that is some other mechanisms. Referring to Fig. 2, for the initial concentrations of 0.8 mg/L, the first stage was completed within the first 2 h, and the second stage of

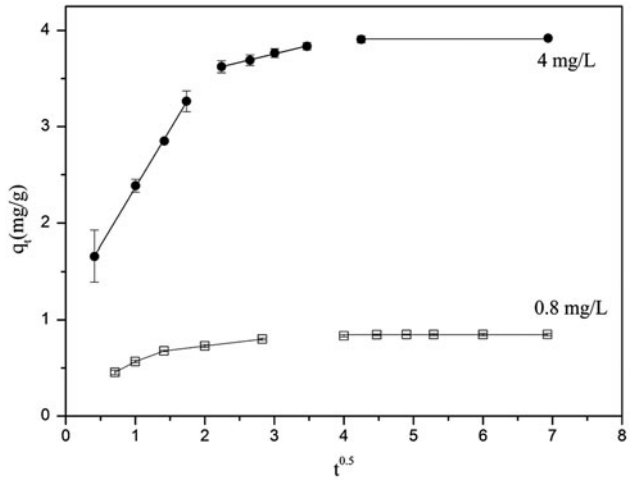

Fig. 2. Plot of q_t vs. $t^{0.5}$.

intra-particle diffusion control was then attained. And the first stage was completed within the first 3 h for the initial concentration of 4.0 mg/L. The values of intercept C_i and the intra-particle diffusion coefficient k_i at different initial concentration are shown in Table 2. The different stages of rates of adsorption observed indicated that the adsorption rate was initially faster and then slowed down when the time increased. Table 2 also shows that the C_i value of the second stage is much greater than that of the first stage for a constant initial SMM concentration. And the C_i value increases with the increase in initial SMM concentration. An increase in C_i value reflects the increase in the thickness of boundary layer, which

Table 2
Intra-particle diffusion parameters

	Intra-particle diffusion					
C_0 (mg/L)	k_{i1} (mg/h$^{0.5}$/g)	C_1	R_1^2	k_{i2} (mg/h$^{0.5}$/g)	C_2	R_2^2
0.8	0.3108	0.2426	0.9783	0.0863	0.5550	0.9999
4.0	1.2035	1.1690	0.9992	0.1757	3.2294	0.9948

decreases the change of external mass diffusion and increases the change of internal mass transfer [26]. Hence, the intra-particle diffusion may also partly control the adsorption process of SMM on CP as well as the film diffusion.

3.2. Effect of solution pH

Solution chemistry often plays an important role in the distribution of organic compounds in solid–liquid systems. The effect of pH on the adsorption of SMM on CP was studied using solutions with initial SMM concentrations of 4.0 mg/L at 298 K at pH 2.0–12.0 (Fig. 3). Clearly, pH was an important parameter that strongly affected the adsorption of SMM onto CP. The maximum adsorption occurred at pH 2.0–6.0. The adsorption capacity could reach about 3.99 mg/g. SMM adsorption decreased with further increase in pH (from 6.0 to 12.0). At pH 12.0, the adsorption capacity was only 1.15 mg/g. Adsorption of solute from aqueous phase is generally influenced by the characteristics of both adsorbate and adsorbent. SMM in solution, for instance, is amphoteric and can exist in the dissociated or undissociated forms under various pH conditions. That is, SMM can be cationic, neutral, or anionic depending on the solution pH. SMM possesses an amine group (–SO_2NH–) with pK_{a1} of 2.0 and a sulfonamide group (–NH_2–) with pK_{a2} of 6.0 [27,28]. Thus, SMM is less soluble at pH values between 2.0 and 6.0. As adsorption SMM on CP may occur through hydrophobic interactions, the maximum adsorption occurs between pH 2.0 and 6.0.

3.3. Adsorption thermodynamic study

The adsorption isotherms of SMM on CP at various temperatures are presented in Fig. 4. The isotherms exhibit an increasing trend in the amounts of adsorbed SMM, and linear behaviors are apparent. Linear regression analyses were insufficient for explaining the experimental data while non-linear regression described the experimental systems more accurately [29]. Therefore, the Henry adsorption isotherm and non-linear Freundlich adsorption isotherm were chosen to fit the experimental data and the best-fitted model was determined based on the use of five error functions to calculate the error deviations between the experimental and predicted equilibrium adsorption data. Since the minimization of each of the error functions renders a corresponding set of isotherm parameters, "sum of the normalized errors" function (SNE) was used for selecting the optimum isotherm parameters among them and the best fitted parameters for each isotherm model were determined based on the minimum SNE values. The detailed calculation process was described by Foo and Hameed [30].

The Freundlich isotherm is an empirical equation used to describe heterogeneous systems. It can be applied to multilayer adsorption, with non-uniform distributions of adsorption heat and affinities over the heterogeneous surface. The Freundlich isotherm is given by the following [30]:

$$q_e = K_F C_e^{1/n} \tag{5}$$

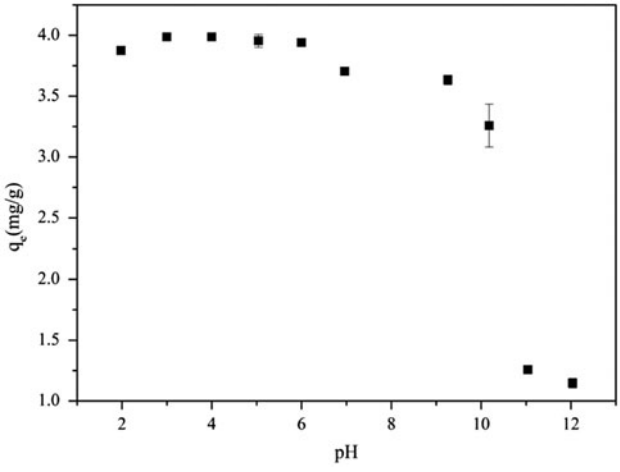

Fig. 3. Adsorption of SMM to CP depending on pH.

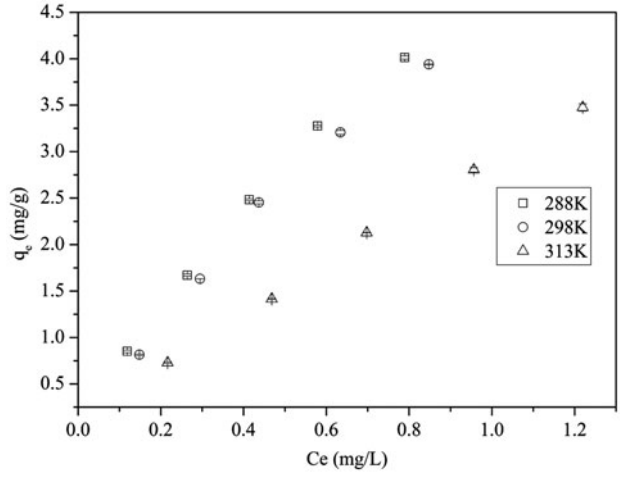

Fig. 4. Adsorption isotherms of SMM onto CP at different temperatures.

where K_F is roughly an indication of the adsorption and $1/n$ of the adsorption intensity.

The Henry isotherm, a linear model for partition, can be described with the following equation:

$$Q_e = K_d C_e \tag{6}$$

where K_d is the Henry constant (L/g)

The sum of the squares of the errors (SSE):

$$\mathrm{SSE} = \sum_{i=1}^{n} (q_{\mathrm{cal}} - q_e)_i^2 \tag{7}$$

The sum of the absolute errors (SAE):

$$\mathrm{SAE} = \sum_{i=1}^{n} |q_e - q_{\mathrm{cal}}|_i \tag{8}$$

The average relative error (ARE):

$$\mathrm{ARE} = \frac{\sum |(q_{\mathrm{cal}} - q_e)/q_e|}{n} \tag{9}$$

The hybrid fractional error function (HYBRID) was developed by Porter et al. in order to improve the fit of the SSE [31]:

$$\mathrm{HYBRID} = \frac{1}{n-p} \sum_{i=1}^{n} \left(\frac{(q_e - q_{\mathrm{cal}})^2}{q_e} \right)_i \tag{10}$$

Merquardt's percent standard deviation (MPSD):

$$\mathrm{MPSD} = \sqrt{\frac{1}{n-p} \sum_{i=1}^{n} \left(\frac{q_e - q_{\mathrm{cal}}}{q_e} \right)_i^2} \tag{11}$$

where n is the number of experimental data points, q_{cal} is the predicted (calculated) quantity of SMM adsorbed according to the isotherm equations, and q_e is the experimental data.

Freundlich and Henry model parameters were evaluated by a non-linear regression method by minimizing error functions and the optimum isotherm constants obtained using the different error functions are presented in Tables 3 and 4. Values of SNE were used to assess best error function for selecting the

Table 3
SNE and error function values for Freundlich isotherm models at different temperatures

Temperature (K)		SSE	SAE	ARE	HYBRID	MPSD
288	K_F	4.9282	4.9283	4.8492	5.1424	4.9874
	n	1.2548	1.2547	1.2500	1.1839	1.2244
	SSE	**0.0183**	0.0298	0.0429	0.0207	0.0258
	SAE	0.287	**0.2662**	0.2754	0.2754	0.2719
	ARE	0.0287	0.0236	**0.0154**	0.0218	0.0182
	HYBRID	0.0027	0.0036	0.0037	**0.0022**	0.0025
	MPSD	0.0427	0.0392	0.0309	0.0299	**0.0273**
	SNE	4.1563	4.3355	4.2198	**3.4965**	3.4980
298	K_F	4.6132	4.5273	4.5273	4.7120	4.8294
	n	1.1997	1.1975	1.1975	1.1427	1.0986
	SSE	0.0448	0.0582	0.1167	0.0548	0.0816
	SAE	0.4280	0.4056	0.5431	0.4365	0.4893
	ARE	0.0531	0.0482	0.0389	0.0426	0.0402
	HYBRID	0.0099	0.0105	0.0125	0.0078	0.0092
	MPSD	0.0953	0.0887	0.0661	0.0676	0.0600
	SNE	3.9640	3.9240	4.4262	**3.4089**	3.7228
313	K_F	2.9105	2.9051	2.9202	2.9103	2.9062
	n	1.0961	1.1074	1.1032	1.0947	1.0985
	SSE	0.0031	0.0037	0.0036	0.0031	0.0032
	SAE	0.106	0.0958	0.0945	0.1079	0.1039
	ARE	0.0128	0.0122	0.0106	0.0131	0.0126
	HYBRID	0.0007	0.0008	0.0008	0.0006	0.0007
	MPSD	0.0204	0.0235	0.0224	0.0205	0.0204
	SNE	4.5404	4.8192	4.6111	**4.4602**	4.5327

Table 4
SNE and error function values for Henry isotherm models at different temperatures

Temperature (K)		SSE	SAE	ARE	HYBRID	MPSD
288	k_H	5.4674	5.6593	5.9987	5.6248	5.8915
	SSE	**0.2437**	0.2884	0.5861	0.2738	0.4619
	SAE	1.0606	**0.9480**	1.142	0.9682	1.0807
	ARE	0.1139	0.0968	**0.0906**	0.0999	0.0926
	HYBRID	0.0414	0.0383	0.0561	**0.0382**	0.0473
	MPSD	0.172	0.1537	0.1470	0.1563	**0.1451**
	SNE	4.0825	**3.7484**	4.6501	3.7817	4.2342
298	k_H	4.9628	5.0591	5.5074	5.0722	5.2183
	SSE	**0.1907**	0.2039	0.6118	0.2077	0.2834
	SAE	0.8617	**0.7976**	1.0674	0.8055	0.8934
	ARE	0.0811	0.0710	**0.0596**	0.0707	0.0669
	HYBRID	0.0259	0.0241	0.0534	**0.0241**	0.0274
	MPSD	0.114	0.1027	0.1187	0.1015	**0.0949**
	SNE	3.5644	3.2725	4.7349	**3.2723**	3.4377
313	k_H	2.9246	2.9325	3.0235	2.9607	3.0263
	SSE	**0.0277**	0.0279	0.0585	0.0318	0.0603
	SAE	0.3300	**0.3212**	0.3935	0.3436	0.3983
	ARE	0.0471	0.0456	**0.0408**	0.0441	0.041
	HYBRID	0.0068	0.0066	0.0078	**0.0063**	0.008
	MPSD	0.0836	0.0819	0.0715	0.0767	**0.0715**
	SNE	4.1379	4.0419	4.6546	**4.0313**	4.7258

isotherm model and calculating parameters. Figures in bold type indicate the minimum values of SNE for relevant error function. In the case of the Freundlich and Henry model, non-linear regression with error functions reveals differences in the values of isotherm constants. From the tables, the results suggest that a lower absolute error value was generally obtained for the Freundlich isotherms at different temperatures. This shows that the Freundlich model exhibited a better fit for the isotherm data. According to the values in Table 3, HYBRID provided the best estimation of parameters for the Freundlich models due to it having the lowest SNE values. So the HYBRID error function was selected for evaluating the fitting of the Freundlich isotherm model to experimental data. The values of n and K_F in these columns are the optimum isotherm constants at different temperatures. In addition, higher temperatures lead to smaller values of the adsorption capacity and K_F. Therefore, low temperature is conducive to the adsorption of SMM on CP. Since equilibrium data were characterized by the Freundlich isotherm model, the thermodynamic parameters, such as enthalpy change (ΔH), Gibbs free energy change (ΔG), and entropy change (ΔS), can be estimated with the following equations [32]:

$$\Delta G = -RT \ln K_0 \tag{12}$$

$$\Delta G = \Delta H - T\Delta S \tag{13}$$

then:

$$\ln K_0 = -\Delta H/RT + \Delta S/R \tag{14}$$

where ΔG (kJ/mol) is the free energy of adsorption; ΔH (kJ/mol) is the apparent enthalpy of adsorption; ΔS (J/K mol) is the entropy of adsorption; R is the universal gas constant (8.314 J/mol K), T is the absolute temperature (K), and K_0 is the thermodynamic equilibrium constant. Values of K_0 are obtained by plotting $\ln(C_s/C_e)$ vs. C_s and extrapolating C_s to zero. Values of ΔH and ΔS can be determined from the slopes and the intercept of the plot between $\ln K_0$ and $1/T$.

Then the predicted thermodynamic constants shown in Table 5 can be determined through linearization of the test data, as shown in Fig. 5. The values of ΔG are negative at all temperatures and they become

Table 5
The thermodynamic properties from adsorption of SMM on CP

Temperature (K)	Enthalpy (ΔH) (kJ/mol)	Entropy (ΔS) (J/Kmol)	Free energy change (ΔG) (kJ/mol)
288			−1.7833
298	−15.5630	−47.8462	−1.3048
318			−0.5871

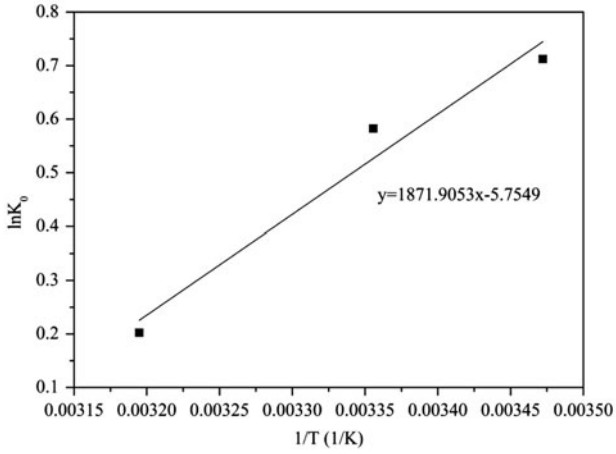

Fig. 5. Plot of $\ln K_0$ vs. $1/T$ for adsorption of SMM on CP.

less negative as the temperature increases. Negative values of ΔG show the spontaneous nature of the sorption processes. The negative value for ΔH indicates that the adsorption was an exothermic process. The negative value of ΔS indicated a greater stability of the adsorption process and the adsorbed SMM is in a stable arrangement and a more ordered form [33]. This indicates increased randomness at the solid–liquid interface during the sorption process and also indicated that the process is entropy driven and not enthalpy driven [34]. Bonding strengths of <84 kJ/mol are typical of physisorption bonds. In contrast, chemisorption bond strengths can range from 84 to 420 kJ/mol [35]. Therefore, binding of SMM on CP is physisorption. Additionally, entropy and enthalpy changes for hydrophobic adsorption have negative values [36].

4. Conclusions

The present work shows that CP can be used as an effective adsorbent for SMM removal from aqueous solutions. The uptake of SMM on CP increases as the initial SMM concentration increases. High pH is unfavorable for the adsorption of SMM on CP. Utilizing pseudo-second-order equation provides the best correlation for all of the adsorption processes. Pseudo-first-order equations do not give a good fit to the experimental data for the adsorption of SMM. The diffusion simulation shows that the intra-particle diffusion is not the only rate-limiting step. Comparison of the Henry isotherm and Freundlich models was performed using five error functions and the SNE procedure was used to select the best error function. The Freundlich model performed better for the equilibrium data. The HYBRID function provided the lowest SNE values and was used to obtain isotherm parameters. The influence of temperature on adsorption is significant; in particular, low temperature is conducive to adsorption. The adsorption is an exothermic process, and negative values of entropy and enthalpy changes verified this adsorption of SMM on CP via hydrophobic adsorption. Additionally, the observed effects of pH on adsorption show that the adsorption of SMM on CP is strongest at about pH 2.0–6.0, and that an alkaline environment inhibits adsorption.

Acknowledgment

We express sincere gratitude to the National Natural Science Foundation of China (20907058) for financial support in this research.

References

[1] A.K. Sarmah, M.T. Meyer, A.B. Boxall, A global perspective on the use, sales, exposure pathways, occurrence, fate and effects of veterinary antibiotics (VAs) in the environment, Chemosphere 65 (2006) 725–759.
[2] T.A. Ternes, A. Joss, H. Siegrist, Peer reviewed: Scrutinizing pharmaceuticals and personal care products in wastewater treatment, Environ. Sci. Technol. 38 (2004) 392A–399A.
[3] D.W. Kolpin, E.T. Furlong, M.T. Meyer, E.M. Thurman, S.D. Zaugg, L.B. Barber, H.T. Buxton, Pharmaceuticals, hormones, and other organic wastewater contaminants in US streams, 1999−2000: A national reconnaissance, Environ. Sci. Technol. 36 (2002) 1202–1211.
[4] N. Watanabe, B.A. Bergamaschi, K.A. Loftin, M.T. Meyer, T. Harter, Use and environmental occurrence of antibiotics in freestall dairy farms with manured forage fields, Environ. Sci. Technol. 44 (2010) 6591–6600.
[5] S. Ye, Z. Yao, G. Na, J. Wang, D. Ma, Rapid simultaneous determination of 14 sulfonamides in wastewater by liquid chromatography tandem mass spectrometry, J. Sep. Sci. 30 (2007) 2360–2369.
[6] R. Hirsch, T. Ternes, K. Haberer, K. Kratz, Occurrence of antibiotics in the aquatic environment, Sci. Total Environ. 225 (1999) 109–118.
[7] D. Zhang, B. Pan, H. Zhang, P.L. Ning, B. Xing, Contribution of different sulfamethoxazole species to their overall adsorption on functionalized carbon nanotubes, Environ. Sci. Technol. 44 (2010) 3806–3811.
[8] M. Kahle, C. Stamm, Sorption of the veterinary antimicrobial sulfathiazole to organic materials of different origin, Environ. Sci. Technol. 41 (2007) 132–138.
[9] M. Kahle, C. Stamm, Time and pH-dependent sorption of the veterinary antimicrobial sulfathiazole to clay minerals and ferrihydrite, Chemosphere 68 (2007) 1224–1231.
[10] L. Ji, W. Chen, S. Zheng, Z. Xu, D. Zhu, Adsorption of sulfonamide antibiotics to multiwalled carbon nanotubes, Langmuir 25 (2009) 11608–11613.

[11] S.F. Yang, C.F. Lin, A. Yu-Chen Lin, P.-K. Andy Hong, R.A. Hong, Sorption and biodegradation of sulfonamide antibiotics by activated sludge: Experimental assessment using batch data obtained under aerobic conditions, Water Res. 45 (2011) 3389–3397.
[12] F. Ogata, H. Tominaga, M. Kangawa, K. Inoue, N. Kawasaki, Removal of sulfa drugs by sewage treatment in aqueous solution systems: Activated carbon treatment and ozone oxidation, J. Oleo Sci. 61 (2012) 217–225.
[13] J. Gao, Adsorption of sulfonamide antimicrobial agents to clay minerals, Environ. Sci. Technol. 39 (2005) 9509–9516.
[14] J. Lagona, P. Mukhopadhyay, S. Chakrabarti, L. Isaacs, The cucurbit[*n*]uril family, Angew. Chem. Int. Ed. 44 (2005) 4844–4870.
[15] W.A. Freeman, W.L. Mock, N.Y. Shih, Cucurbituril, J. Am. Chem. Soc. 103 (1981) 7367–7368.
[16] L. Liu, N. Zhao, O.A. Scherman, Ionic liquids as novel guests for cucurbit[6]uril in neutral water, Chem. Commun. 9 (2008) 1070–1072.
[17] S. Karcher, A. Kornmüller, M. Jekel, Removal of reactive dyes by sorption/complexation with cucurbituril, Water Sci. Technol. 40 (1999) 425–433.
[18] S. Karcher, A. Kornmüller, M. Jekel, Cucurbituril for water treatment. Part I, Water Res. 35 (2001) 3309–3316.
[19] T. Jin, D. Chen, Y. Liu, Y. Dong, H. Qiao, X. Chen, Preparation of cucurbit[6]uril anchored silica gel and its adsorption characteristics of sulfamonomethoxine, Acta Sci. Circumst. 33 (2013) 991–996 (in Chinese).
[20] H.T. Qiao, P. Wang, Y. Liu, Y.H. Dong, T. Jin, X.L. Chen, C.C. Si, Synthesis of polymer cucurbituril with microwave electrodeless lamp and its absorption properties of dye, New Chem. Mater. 41 (2013) 82–84 (in Chinese).
[21] S.Y. Jon, N. Selvapalam, D.H. Oh, J.K. Kang, S.Y. Kim, Y.J. Jeon, J.W. Lee, K. Kim, Facile synthesis of cucurbit[*n*]uril derivatives via direct functionalization: Expanding utilization of cucurbit[*n*]uril, J. Am. Chem. Soc. 125 (2003) 10186–10187.
[22] A. Day, A.P. Arnold, R.J. Blanch, Controlling factors in the synthesis of cucurbituril and its homologues, J. Org. Chem. 66 (2001) 8094–8100.
[23] S. Lagergren, Zur theorie der sogenannten adsorption geloester stoffe, K. Svenska Vetenskapsakad. Handl. 24 (1989) 1–39.
[24] B. Cheng, Y. Le, W. Cai, J. Yu, Synthesis of hierarchical $Ni(OH)_2$ and NiO nanosheets and their adsorption kinetics and isotherms to Congo red in water, J. Hazard. Mater. 185 (2011) 889–897.
[25] W.J. Weber, J.C. Morris, Kinetics of adsorption on carbon from solution, J. San. Eng. Div. 89 (1962) 31–39.
[26] X. Han, W. Wang, X. Ma, Adsorption characteristics of methylene blue onto low cost biomass material lotus leaf, Chem. Eng. J. 171 (2011) 1–8.
[27] C.E. Lin, C.C. Chang, W.C. Lin, Migration behavior and separation of sulfonamides in capillary zone electrophoresis II. Positively charged species at low pH, J. Chromatogr. A 759 (1997) 203–209.
[28] T. Li, Z.G. Shi, M.M. Zheng, Y.Q. Feng, Multiresidue determination of sulfonamides in chicken meat by polymer monolith microextraction and capillary zone electrophoresis with field-amplified sample stacking, J. Chromatogr. A 1205 (2008) 163–170.
[29] A. Gunay, Application of nonlinear regression analysis for ammonium exchange by natural (Bigadiç) clinoptilolite, J. Hazard. Mater. 148 (2007) 708–713.
[30] K.Y. Foo, B.H. Hameed, Insights into the modeling of adsorption isotherm systems, Chem. Eng. J. 156 (2010) 2–10.
[31] J.F. Porter, G. McKay, K.H. Choy, The prediction of sorption from a binary mixture of acidic dyes using single- and mixed-isotherm variants of the ideal adsorbed solute theory, Chem. Eng. J. 54 (1999) 5863–5885.
[32] R. Niwas, U. Gupta, A.A. Khan, K.G. Varshney, The adsorption of phosphamidon on the surface of styrene supported zirconium(IV) tungstophosphate: A thermodynamic study, Colloids Surf., A: Physicochem. Eng. Asp. 164 (2000) 115–119.
[33] D. Xu, X.L. Tan, X.K. Chen, X.K. Wang, Adsorption of Pb(II) from aqueous solution to MX-80 bentonite: Effect of pH, ionic strength, foreign ions and temperature, Appl. Clay Sci. 41 (2008) 37–46.
[34] Y. Shih, Y. Su, R. Ho, P. Su, C. Yang, Distinctive sorption mechanisms of 4-chlorophenol with black carbons as elucidated by different pH, Sci. Total Environ. 433 (2012) 523–529.
[35] Y.S. Al-Deg, M.I. El-Barghouthi, H. El-sheikh, G.M. Walker, Effect of solution pH, ionic strength, and temperature on adsorption behavior of reactive dyes on activated carbon, Dyes Pigm. 77 (2008) 16–23.
[36] B.K. Głód, P.W. Alexander, Z.L. Chen, P.R. Haddad, Thermodynamic investigation of sample retention mechanism in ion-exclusion chromatography with inclusion compound in the mobile phase, Anal. Chim. Acta 306 (1995) 267–272.